Behavior of Kinesin Driven Quantum Dots Trapped in a Microtubule Loop

Aurélien Sikora,[†,○] Filippo Federici Canova,[†] Kyongwan Kim,[†] Hikaru Nakazawa,[‡] Mitsuo Umetsu,[‡] Izumi Kumagai,[‡] Tadafumi Adschiri,[†] Wonmuk Hwang,[§,⊥,∥] and Winfried Teizer*[,†,∥,#]

[†]WPI Advanced Institute for Materials Research, Tohoku University, 2-1-1 Katahira, Sendai 980-8577, Japan, [‡]Department of Biomolecular Engineering, Graduate School of Engineering, Tohoku University, Sendai 980-8579, Japan, [§]Department of Biomedical Engineering, Texas A&M University, College Station, Texas 77843-3120, United States, [⊥]School of Computational Sciences, Korea Institute for Advanced Study, Seoul 130-722, Korea, [∥]Materials Science and Engineering, Texas A&M University, College Station, Texas 77843-3003, United States, and [#]Department of Physics and Astronomy, Texas A&M University, College Station, Texas 77843-4242, United States [○]Present address: Laboratoire Lasers Plasmas et Procédés Photoniques (LP3) , Case 917, 163 Avenue de Luminy, Marseille 13009, France.

ABSTRACT We report the observation of kinesin driven quantum dots (QDs) trapped in a microtubule loop, allowing the investigation of moving QDs for a long time and an unprecedented long distance. The QD conjugates did not depart from our observational field of view, enabling the tracking of specific conjugates for more than 5 min. The unusually long run length and the periodicity caused by the loop track allow comparing and studying the trajectory of the kinesin driven QDs for more than 2 full laps, *i.e.*, about 70 μm, enabling a statistical analysis of interactions of the same kinesin driven object with the same obstacle. The trajectories were extracted and analyzed from kymographs with a newly developed algorithm. Despite dispersion, several repetitive trajectory patterns can be identified. A method evaluating the similarity is introduced allowing a quantitative comparison between the trajectories. The velocity variations appear strongly correlated to the presence of obstacles. We discuss the reasons making this long continuous travel distances on the loop track possible.

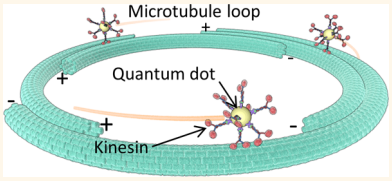

KEYWORDS: quantum dots · kinesin · microtubules · motor proteins · molecular transport

Intracellular delivery of cargos is achieved by sophisticated motor proteins. In axons, with the use of multiple motors attached to the cargo and multiple tracks,[1] the range of transportation can reach many centimeters.[2] Among those motors, kinesin-1, hereafter referred to as kinesin, is characterized by its high processivity, *i.e.*, its ability to stay attached on its track after each 8 nm displacement. Kinesin walks along a biopolymer track, the microtubule (MT), a hollow tube formed by 13 protofilaments, depending on the polymerization conditions.[3] The MT is characterized by the different growth rate of its minus (slow) and plus end (fast).[4] Kinesin moves toward the plus end and follows the same protofilament.[5] Yet, sideways steps can occur occasionally.[6] *In vivo*, kinesin navigates in a highly crowded environment and encounters many obstacles on its way. It has been shown *in vitro* that kinesin can stay attached and waits until the obstacle leaves,[7] can detach or bypass it.[8,9] Despite its high processivity, kinesin eventually detaches after an average distance of about 1 μm.[10] This limits its application for long-range transportation. However, the run length can be increased by attaching more motors to the cargo[7,11−13] or by using an array of MTs.[14] Yet, the precise influence of the number of MTs on the traveled distance is not known. Stochastic simulations show that the traveled distance increased exponentially with the number of bound motors.[15] Theoretically, 7 motors working cooperatively are enough to reach a traveled distance in the centimeter range.[16] Experimentally, the precise effect of the number of motor per cargo seems unclear. For example, with 20 kinesins per cargo, a resulting running length of only a few micrometers has been reported.[17] Yet, in this configuration, the number of kinesins pulling together is not known. In parallel, a significant increase of run length (more than 8 μm with 2 motors) has been measured.[18] In this experiment, the number of motors is determined by measuring the stall force. To be certain of the number of pulling motors, it is also possible to use a special antibody or a DNA scaffold which binds to only 2 kinesins.[19,20] It resulted in an average

* Address correspondence to teizer@tamu.edu.

Received for review July 14, 2015 and accepted October 1, 2015.

Published online October 01, 2015
10.1021/acsnano.5b04348

walking distance of 3 and 1.4 μm, respectively. In all these assays, the experimental conditions are not fully equivalent. Thus, parameters other than the number of motors are expected to influence the walking distance. For example, the geometry of the kinesin-bead system varies. Different kinesin chain lengths, bead sizes and scaffolds are used. This results in various motor orientations and spatial deformations which may alter the binding rate. In any case, the limited length of a MT does not allow the study of long-range cargo transport. However, by forming loops, the path becomes unlimited in principle. Moreover, this configuration allows the monitoring of the same kinesin driven cargo during consecutive laps. In this way, it becomes possible to compare its behavior from one lap to another. Recently, MT loop formation has been reported.[21−23] One method consists in labeling tubulin with biotin and triggering an active self-organization by inserting streptavidin during a gliding assay.[24] Here, we show that loops can be obtained by controlling surface treatment and flow. As only the glass surface is treated, this method allows to work with clean MT surfaces on which the kinesin binding sites are fully available. Moreover, the surface treatment helps at stabilizing the MT formations, which facilitates the analysis of the motor motion along the loops. Quantum dot (QD) assays performed on these loops resulted in unexpected high running lengths allowing the study of their trajectory for more than 2 laps. Thus, this experiment allows identifying factors that influence the behavior of a kinesin driven object. In this article, the characterization of these trajectories is presented with the aim to quantify the similarities from one lap to another. In the first part, the MT loop and the trajectory acquisition methods will be presented. Then, on the basis of data extracted from the trajectories, the velocities of the kinesin driven QD will be compared. The third part deals with the correlation between visible obstacles and velocity variation. On the basis of these variations, a method aiming at quantifying the similarity between trajectories is presented. Last, we discuss how such long traveled distances can be achieved.

RESULTS AND DISCUSSION

Loop Formation. After MT insertion in the flow cell, closed MT formations were occasionally found on the poly-L-lysine (PLL) treated surface. This positively charged polymer binds to the negatively charged glass surface and to the MT allowing their attachment.[25] During flushing of the flow cell, the weakly attached part of the MT moved with the flow, making them bend. If the MT is long enough and/or in contact with other MTs, loops are occasionally seen to form. The density of closed MT structures, *i.e.*, an assembly of MTs where periodic motion of QDs is possible, is estimated at about 3 mm^{-2} at 2.5 μg mL^{-1} tubulin concentration. It reaches about 23 mm^{-2} at 10 μg mL^{-1}. This density increases upon insertion of kinesin quantum dot conjugates (see Table S1). Thus, the formation of the closed structures is enhanced by the presence of kinesin.

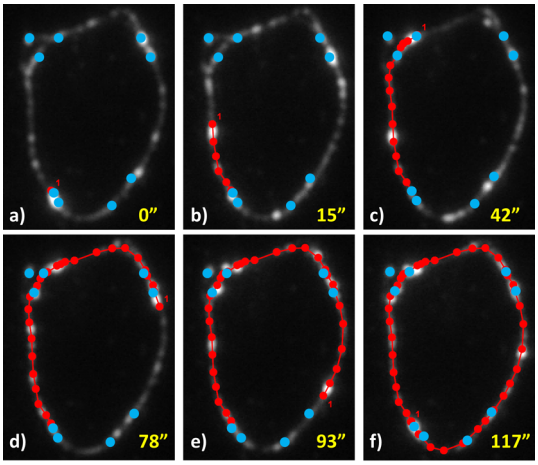

Figure 1. Fluorescence microscopy images showing the quantum dots translocating along the microtubule loop. The tracking of the quantum dot is shown in red. The positions of the quantum dot are marked with red dots. Separation between adjacent markers is 3 s. The brightest immobile quantum dots, identified using a minimum intensity image of the video sequence, are labeled by blue dots. The full perimeter of the loop is 27.8 μm.

At 5 μg mL^{-1} tubulin concentration, numerous loops are incorporated in large MT networks. In this system, the motor covered QDs help linking the MTs. Due to the presence of PLL, active self-assembly is limited. Therefore, the closed MT formations are thought to be mainly caused by the flow during QD insertion. Among 40 studied closed MT structures, almost 50% were found to enable unidirectional QD transport. This corresponds to the probability for a bundle of two MTs to be polarity aligned and would indicate a random formation of loops composed of two MTs. However, in the case of a larger number of MTs, a preferential alignment mechanism is necessary to explain this high probability. While we do not understand the details of this mechanism, the unipolar alignment may be caused by the flow field applied during the insertion of QD conjugates.[26]

QD Assay Performed in a MT Loop. A QD assay was performed on a MT loop. The motion of the QD has been recorded for 5 min, allowing the completion of more than 2 laps (*cf.* Movie S1). Figure 1 shows the tracking of a QD completing one lap, *i.e.*, 27.8 μm, with marker dots along the MT loop. The time between sequential dots is constant (3 s). The distance between sequential dots varies showing the changing speed of the kinesin driven object. The QD seems to slow down, but neither stops nor detaches, when encountering a bright immobile QD obstacle on the track.

The QD trajectories were analyzed using a kymograph performed on the whole loop. The spatial periodicity allows the assembly of several identical kymographs in order to obtain a convenient view of the full QD

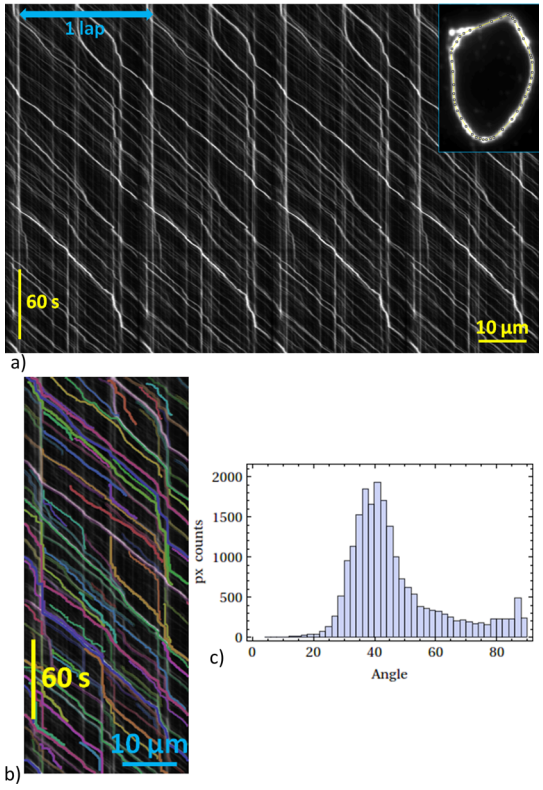

Figure 2. (a) Composite kymograph showing the trajectories of quantum dots along the loop. Inset: fluorescent microscopy image (intensity averaged from 3000 frames) of the microtubule loop showing the selected path used for the kymograph. The length of the path is about 27.8 μm (1 lap). (b) Trajectories detected by the virtual stepper (in color) overlaid on the kymograph acquired along the loop. (c) Histogram showing the distribution of the measured angles on the lines.

trajectories (*cf.* Figure 2a). Vertical lines presumably correspond to QD conjugates in which kinesin has stalled. This may be caused by some deterioration of the motor protein. The trajectories show that moving QDs are sometimes slowed down when encountering a stuck QD. The continuity of the lines points out that the QDs did not leave the tracks. The trajectories present large brightness heterogeneity. Progressive fading due the presence of β-mercaptoethanol[17] and the possibility of clustering may be responsible for this dispersion. Figure S1 displays the distribution of the average intensity of the trajectories. It shows that the majority of the moving objects emit a low intensity light. Accordingly, the clusters constitute a minority of the observable moving QDs. The obstacles do not seem to prevent the motion of the kinesin driven QD. This is consistent with other experiments in which kinesin bypasses obstacles instead of leaving the track.[9] The lines are all oriented from top left to bottom right corner, indicating that the QD are moving in only one direction. Thus, the loop is formed either by a single spiraling MT or by several in unipolar orientation.

The data were extracted by hand and by using a computational approach, which allows reducing acquisition mistakes and makes the process fast and reproducible. This method consists of using a virtual stepper walking along the lines. Its path is determined by the average intensity of the next 3 pixels. It follows always the maximum intensity and blackens its previous step prints (see Materials and Methods for details).

Figure 2b shows the trajectories detected by the virtual stepper. As traveling QDs cross several other QDs along the path, some clustering may happen. To check this, the intensity distribution of the detected trajectories for three different times has been plotted (see Figure S2). The distribution changes slightly over time showing that some brighter objects appear. However, the general shape of the distribution does not change, showing a majority of low intensity trajectories.

The angle distribution measured at each pixel location is displayed in Figure 2c. According to the histogram, the average angle of the detected lines is 40°, which corresponds to a speed of about 265 nm/s. This is lower than previously measured.[27] This can be explained by the presence of obstacles slowing down the cargos[7] and by a crowding effect.[28] As the loop is closed, and due to the unusually long travel distance, kinesin driven cargos do not leave the MT track. At the same time, the loop keeps capturing QD available in the environment, contributing to an increase of the density of QD in the loop.

Study of Kinesin Driven QD Behavior along the Loop. Once trajectories are acquired, comparisons can be made. Figure 3a shows 6 QD trajectories manually acquired that have been analyzed. The selected trajectories were defined by the invariance of their brightness and thickness in the kymograph. As the QDs traveled in a loop, their spatial localization is periodic. Thus, each trajectory can be cut at the end of each lap and transposed to the origin of the plot allowing a direct comparison between each cycle. Figure 3b displays all the trajectories gathered in one single lap. Most of them seem concentrated close to the same path. This reveals qualitatively the similarity between the QD trajectories. The overall speed, given by the slope, does not seem to differ notably between each QD as the trajectories are largely parallel.

Figure 3c shows the trajectories followed during subsequent cycles of each QD. The loop allows comparison between laps. The speed, positions and velocity variations of the QDs are sometimes very similar (QD1 and QD4). Periodic abrupt changes of behavior attributed to the presence of obstacles can be noticed, for example, around 24 μm.

To compare trajectories, velocities were averaged on micrometer long sections. Then, for each micrometer, the velocities have been subtracted between each cycle. The resulted velocity differences are displayed in Table 1.

Considering identical micrometer long sections, the difference of QD average velocities can be as close as a

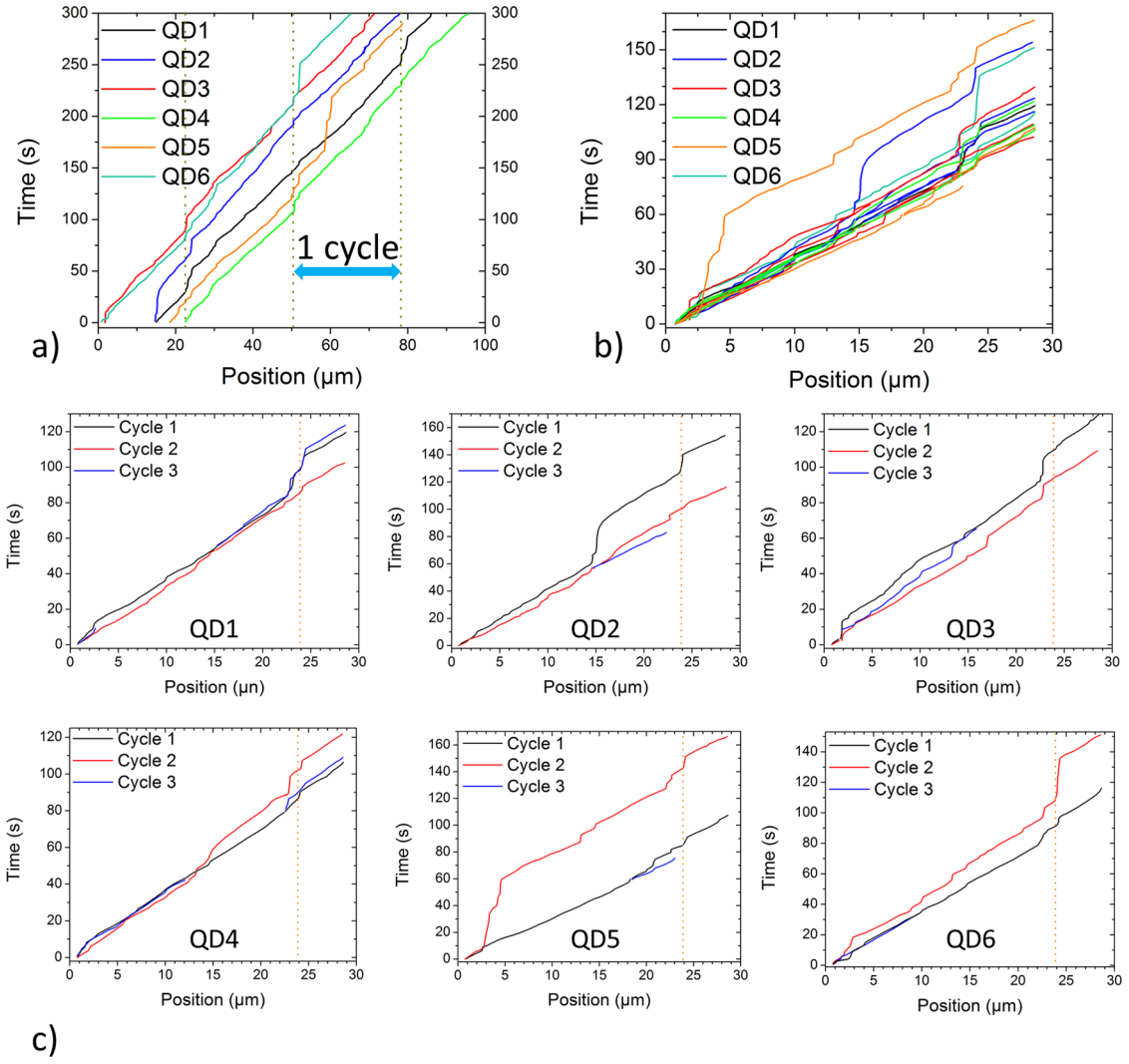

Figure 3. (a) Quantum dot trajectories extracted from the kymograph. The dashed lines indicate a periodic variation of speed. (b) Trajectories gathered in 1 loop cycle. (c) Self-comparison of the quantum dot trajectories. The dotted line indicates one of the positions where the velocity changes abruptly. The length of the selected trajectories varies so they end at different locations.

few nm/s. On average the difference from one lap to another (for the same QD), or from one QD to another is about 75 nm/s, which represent about 25% of the average velocity of the QDs on the loop.

Detailed Analysis of the Velocity Variation. To identify stuck obstacles visible in the loop, we use a minimum intensity profile. Along the loop, this profile keeps only the minimum recorded intensity among all the frames of the video. That way, we eliminate the influence of the bright moving QDs. Figure 4a shows the minimum intensity variation along the loop. The peaks correspond to stuck QDs visible in the kymograph. This intensity profile will serve as a reference for the position of visible obstacles along the loop.

To visualize the influence of the topography on the velocity, a density graph displaying the angle variation as a function of the position has been plotted (Figure 4b). Bright peaks match with the visible obstacles on the loop. Angle fluctuations appear correlated with the variation of the intensity of the profile.

To study the correlation between velocity variation and obstacles, the average velocity has been calculated for each position along the loop. Figure 4c shows the average velocity of all the acquired trajectories in comparison with the minimum intensity profile of the loop. Most of the local velocity minima are correlated with the presence of an obstacle. About 14% of the local minima are above the average velocity. Furthermore, the amplitude of the velocity variation seems more important when the intensity of the peak is large. Figure 4d displays the velocity as a function of the "roughness", *i.e.*, the normalized minimum intensity of the loop (see Figure 4a). The velocity seems to decrease with the "roughness". Assuming a similar brightness within the QD, we can consider that the intensity is correlated to the size of a cluster of immobilized QDs and/or by the QD density on the MT. Thus, this trend can be explained by the longer time necessary to bypass one large or several consecutive obstacles.

TABLE 1. Average Velocity Differences between Cycles

	$V_{C1} - V_{C2}$ (nm/s)			$V_{C1} - V_{C3}$ (nm/s)			$V_{C2} - V_{C3}$ (nm/s)			
	mean ΔV	min ΔV	max ΔV	mean ΔV	min ΔV	max ΔV	mean ΔV	min ΔV	max ΔV	mean ΔV (nm/s)
QD1	70 ± 56	1.8	210	49 ± 39	1.2	130	69 ± 47	1.8	170	63
QD2	60 ± 60	6.8	290	90 ± 82	19	26	67 ± 43	15	140	72
QD3	68 ± 55	6.7	210	91 ± 110	10	360	77 ± 91	6.7	330	79
QD4	80 ± 54	1.9	210	43 ± 37	1.9	130	61	1.9	180	61
QD5	110 ± 86	3.0	300	100 ± 37	64	150	98 ± 80	17	190	100
QD6	62 ± 66	2.8	280	74 ± 90	10	266	62 ± 70	6.2	230	74
AVG	75	3.8	250	75	18	177	72	8.1	210	75

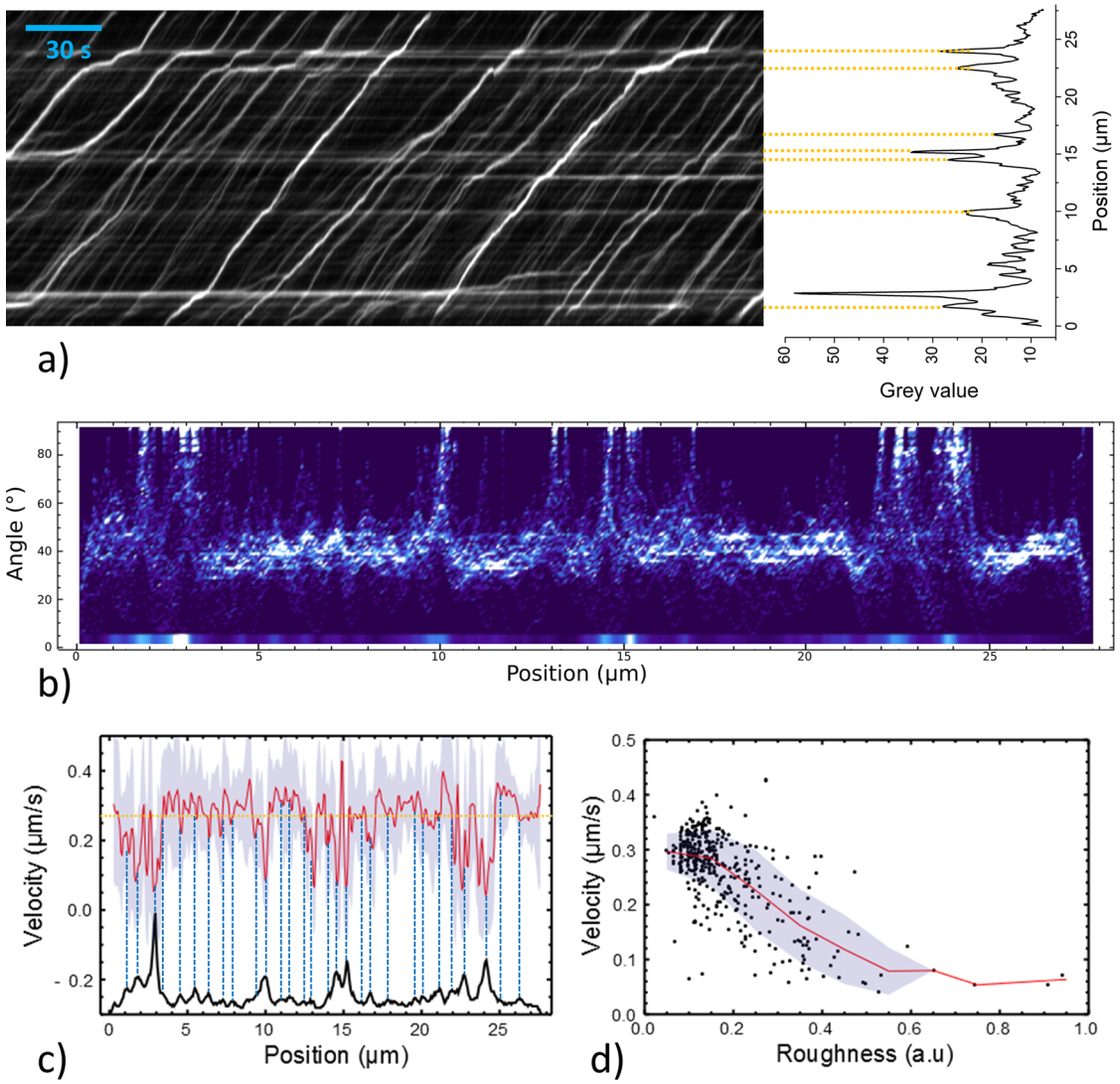

Figure 4. (a) Kymograph and minimum intensity profile of the loop. (b) Density graph of the angle of the lines digitized using the stepper algorithm on the kymograph (*cf.* Figure 2b); 90° corresponds to no motion. The brighter the pixel, the more numerous are the recorded angles. The minimum intensity variation displayed in (a) is represented in a density graph on the bottom. (c) Average velocity extracted from the data acquired using the stepper algorithm in comparison with the minimum intensity profile of the loop. The dashed lines indicate the positions of the obstacles. The dotted line points out the average velocity. (d) Velocity as a function of the "roughness" extracted from the minimum intensity profile. The red line shows the average of the velocity calculated within each 0.1 range of "roughness" values. In both graphs, the shadowed area corresponds to the standard deviation.

The behavior of the kinesin driven QDs has been compared when they encountered a visible obstacle, resulting in three categories of behavior. At the level of the obstacle, the QD's velocity is either locally minimized, decreasing or increasing. Figure 5 shows the velocity variation of QD1 and QD4 in comparison

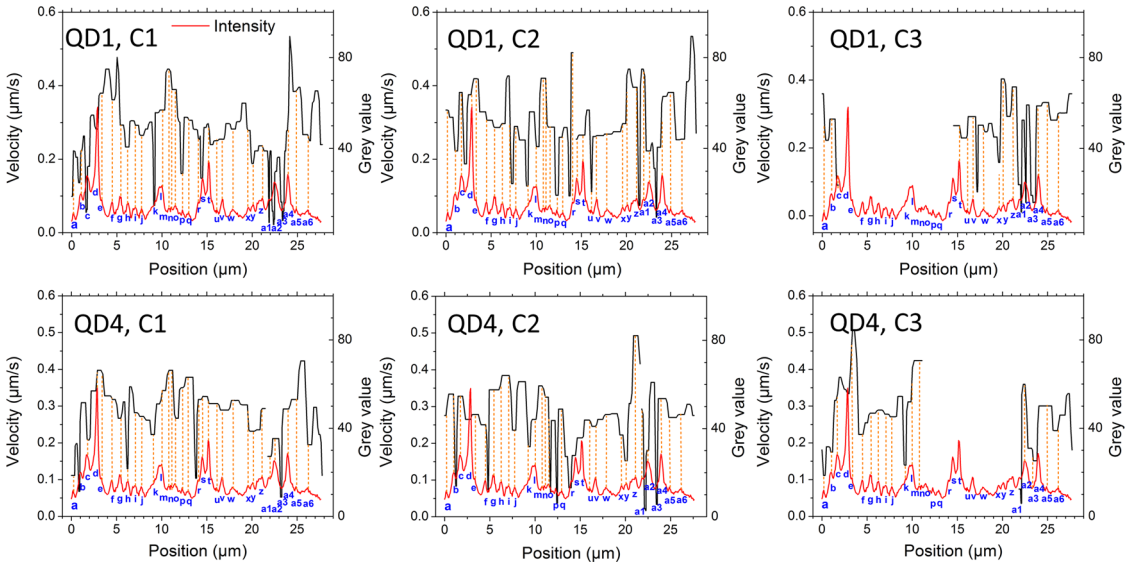

Figure 5. Velocity (black line) as a function of the position on the loop for the three cycles of the QD 1 and 4. The minimum intensity profile along the loop is shown in red and each visible obstacle on the loop is labeled in blue. The green dashed lines indicate the positions of the obstacles.

TABLE 2. For Each Mode of Trajectory Acquisition, Average Behavior, Average Similarity and Corresponding Average Probability of Finding the Same Similarity[a]

acquisition	minimum (%)	↓ (%)	↑ (%)	probability (%)	similarity (%)
manual	28	47	25	11 ± 9.0	50 ± 16
algorithm	46	32	23	14 ± 7.2	38 ± 11

[a] Individual data for QD1 to 6 are available in Table S3.

TABLE 3. Minimal Similarity between Cycles in the Case of 32 and 9 Common Defects, Number of Comparisons, Proportion of Comparisons Presenting a Higher Similarity, and Probability To Get More than This Similarity

N	similarity	number of comparisons	proportion (%)	$P(i > q)$ (%)
32	40	6	100	14
9	33	4	100	35

with the labeled visible defects. Each cycle is characterized by the number of minima, decreasing and increasing points. The data for QD1 and 4 are available in Table S2 and the averaged results are displayed in Table 2. Knowing this behavior for each QD, it is possible to compare the cycles and enumerate the number of similitudes. For each cycle comparison, a similarity index, defined by the ratio between the number of similitudes q and the number of common defects N, can then be calculated. Similitudes can occur for a random behavior. Thus, the probability $P(q,N)$ to get q similitudes in N locations has been calculated (see Materials and Methods for details), allowing us to know if such a similarity is likely to occur.

When encountering an obstacle, the velocity seems to be predominantly either minimized (locally) or in a decreasing phase. Visible obstacles do not necessarily impose a dramatic decrease of the velocity (about 25% of the events). Both acquisition methods show that the trajectories are highly similar. Certain comparisons have the same number of common defects (N). Thus, we can estimate the proportion of comparisons for which their similarity is higher than a given value and compare that to the probability of occurrence in a random behavior. For example, there are 6 comparisons with 32 common defects (*cf.* Table S3). Each of these comparisons has more than 40% similarity. However, for this amount of common defects, the probability $P(I > q)$ to get more than 40% similarity is about 14%. Table 3 shows the similarities and the occurring probabilities in the case of 9 and 32 common defects. For 32 (9) common defects, the probability to get respectively more than 40% (33%) similarity reaches 14% (35%). Yet, 100% of the comparisons display a higher similarity than 40% (33%). For both 32 and 9 common defects, the measured probability (100%) is much higher than the calculated one (14 or 35%). Therefore, the similarity between trajectories does not result from a random behavior.

Run Length. In our experiment, the traveled distance achieved by the kinesin driven QDs reaches at least 70 μm (end of recording). Such a distance cannot be achieved with a single-MT QD assay. One lead susceptible to explain that phenomenon is the number of kinesins per cargo. In this experiment, the ratio is estimated to about 8 motors per cargo, based on the molar concentrations. A similar experiment showed that for a ratio of 6, the run length reaches about 3 μm.[7] According to the extrapolation of these data, at least 24 motors are required to attain 70 μm (see Figure S3a). Yet, the surface of the QD allows a maximum of 10 streptavidins. Assuming that

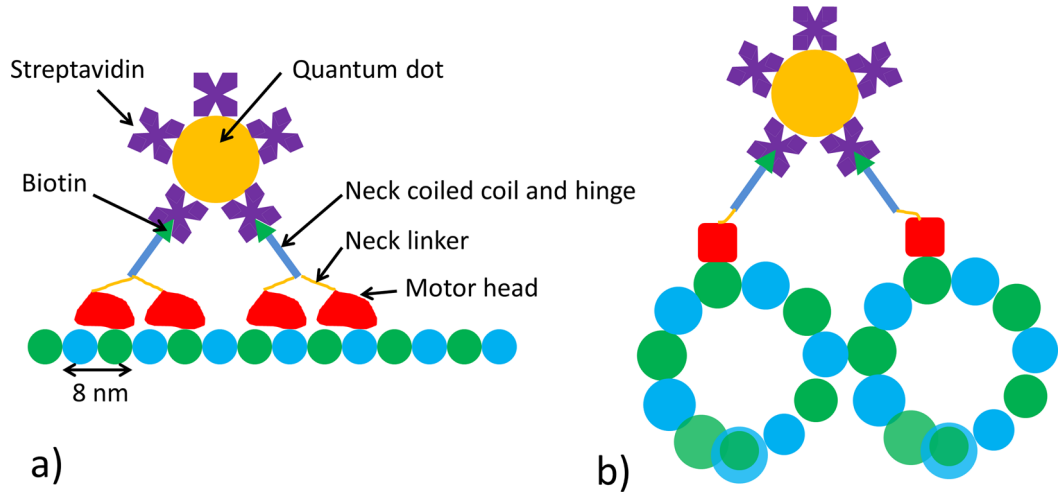

Figure 6. Schematic of the kinesin driven QD bound to one MT (a) or two MTs (b). Dimensions are based on information from the literature and the QD provider.[6,42−44]

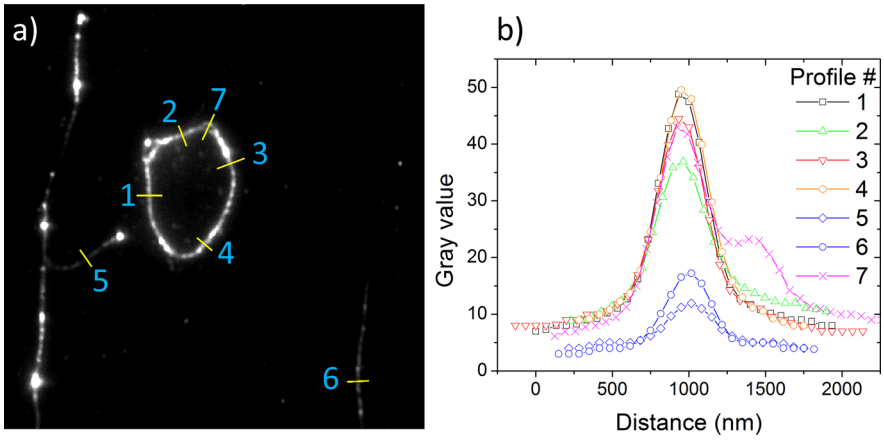

Figure 7. (a) Minimum intensity image extracted from the recorded video sequence. Profiles shown in (b) are represented by yellow lines. Contrast and luminosity have been adjusted to enhance the visibility. (b) Intensity profiles extracted from (a); 5 and 6 are assumed to be profiles of single microtubule (see text) and are considered as references. The parameters extracted from the Gaussian fits are available in Table S4.

only 1 site on 4 per streptavidin is available for kinesin binding due to the geometrical configuration, these QD cannot allow the binding of 24 motors.

Cooperative transport can also be considered. In this case, the motors, if they are able to bind to the MT simultaneously, work together. This has been modeled using two main methods. In the first one, the transition rate model, it is assumed that the motors share the load equally.[16] In the second method, the run length of the multimotor driven cargo is estimated using a stochastic approach.[29] In both cases, 5 motors should allow a run length exceeding 70 μm (see Figure S3b). However, the small size of the QD and the short length of the truncated kinesin barely allow simultaneous binding of 2 motors (see Figure 6a). A third motor cannot reach the microtubule surface. Thus, cooperative transport cannot fully explain the high run length measured in this system.

Another way to increase the apparent run length consists in widening the microtubule track.[14] As the top right and left-hand of the loop show at least 2 MT, the loop is surely formed by several MT. The resolution of the microscope does not allow us to distinguish adjacent MTs. Yet, it is possible to exploit the light intensity in order to estimate the number of MTs. Therefore, the intensity has been measured at different spots of the loop and compared with the signal where the MT is thought to be single, due to their low intensity and the unidirectional transport of QD along them. Figure 7a displays the locations of the different intensity profile realized in these spots. A minimum intensity image of the video sequence is used in order to eliminate the signal of moving or blinking QDs. The profiles are plotted in Figure 7b. The measured intensity is much higher in the loop than for the MT references, confirming the presence of a bundle. Assuming that the intensity increases linearly with the number of (nonsuperposed) MTs, it is possible to estimate their number. On average, the intensity in the bundle is about 3 times the intensity from the reference, indicating that the loop might be formed by 3 MTs.

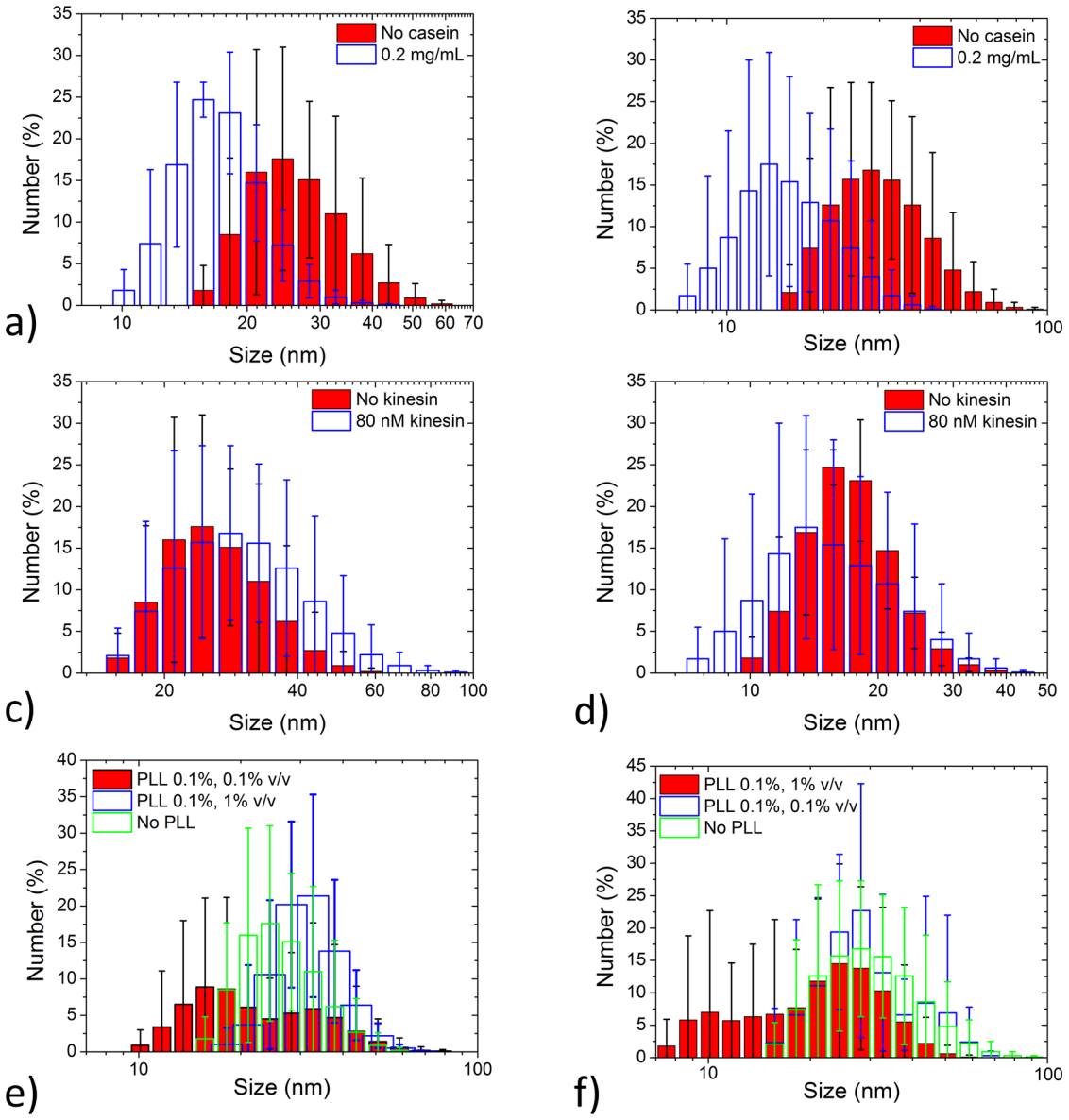

Figure 8. Size distributions measured by DLS. The sample is composed of 1 nM QD diluted in PEM buffer and mixed with casein (a, b, and d), 80 nM kinesin (b–d, and f) and PLL (e and f). Error bars represent the standard deviation based on 5 measurements.

Considering the possibility of QD clustering, multimotor transport is conceivable. For example, a cluster of 3 QDs in diameter will allow 6 simultaneous kinesin bindings on a single MT and therefore would be enough to enable long run lengths. Movie S1 shows large moving asymmetric objects that presumably are constituted by several QDs. Nevertheless, they seem to represent a minority of the visible kinesin driven objects. Dynamic Light Scattering (DLS) experiments on QD solutions have been performed in order to check this observation. Moreover, we tried to identify what could be responsible for the clustering. Thus, we compared the size distribution in the presence of kinesin, casein and PLL. The QDs alone show a size distribution between 15 and 60 nm with a maximum near 25 nm (Figure 8a). According to the manufacturer, the individual size should be distributed around 20 nm. Thus, it confirms that most of the objects are constituted of a single QD, while it does not exclude the presence of small clusters (2 to 3 QDs in diameter). The addition of casein seems to reduce the size (Figure 8a,b). As this protein is well-known to inhibit protein adsorption,[30] this is consistent with expectations. The addition of kinesin slightly increases the size as expected for a QD grafted with proteins (Figure 8c). However, we observed a widening of the size distribution in the presence of casein (Figure 8d). The small diameter objects are presumably constituted by casein micelles.[31] The increase of the size, nonetheless, does not seem significant. We also tested the effect of PLL, a highly cationic polymer susceptible to bind to negatively charged proteins. Its contribution is not clear as we observed both an increase and a decrease of the size distribution depending on the PLL concentration

(Figure 8e,f). However, regardless of the composition of the solution, the size distribution does not exceed 100 nm.

MT loops allow the comparison of trajectories giving access to the motion mechanisms of kinesin driven QDs. The results show that the velocity is correlated with the topography. Within 2 cycles, the velocity difference can be as low as a few and as large as a few hundred nanometers per second (nm/s). In the same manner, at the level of a given obstacle, the kinesin driven cargo can accelerate or decelerate. This may be explained by a change of path. A bundle of MTs offers several available protofilaments allowing the kinesin driven QDs to switch during travel.

The proportion of comparisons presenting high similarity exceeds the level expected for a random trajectory. It confirms the influence of the topography on the behavior of the kinesin driven QD. It would be interesting to check if the similarity increases in the case of a track offering less possible paths along the loop.

A bundle formed by a few MTs seems sufficient to achieve long traveled distances of kinesin driven cargos. In the case of a MT array, this is caused by the possibility for a large cargo to bind simultaneously to several MTs, decreasing the chance of complete unbinding.[14] In this loop experiment, the small diameter of the QD (about 20 nm) and the short length of the kinesin may allow only the simultaneous binding with 2 MTs (*cf.* Figure 6b). A third one may be involved if the MTs are packed in a specific configuration, although it is unlikely that this specific packing is maintained along the whole loop. According to the geometrical constraints, and assuming that the kinesin is flexible enough, a total of 4 kinesins may attach simultaneously to 2 MTs. With 4 motors, the run length reaches in theory 65 μm.[16] This configuration seems insufficient for travel length in excess of 70 μm. Therefore, other factors should be considered.

According to the cooperative transport model, the run length depends on the binding rate of the kinesin, a parameter "difficult to measure".[16] This parameter affects dramatically the average run length (*cf.* Figure S6). In the case of 4 motors, a slight increase is enough to exceed 70 μm. Thus, the high run length measured in this experiment can be explained assuming that the cargo can be pulled simultaneously by 4 motors and by adjusting slightly the mean-field model. A longer recording of the phenomenon will allow the validation of this theory.

The apparent long run length might be composed of several shorter runs, which is more in accordance with the theory. To keep its motion, the kinesin driven QD has to eventually switch from one MT to another. This is unavoidable when it reaches a MT end. A QD assay performed on a bundle of antiparallel MTs shows this phenomenon (*cf.* Movie S2 and Figure S4). The average distance traveled between each MT switch (about 1 μm) is more in accordance with the theory and the reported measurements[7] in the case of a low ratio between kinesin motors and QD ($\sim$1 under the experimental conditions of Movie S2). The maintenance of the close range may be explained by electrostatic interactions.[32]

The achievement of long travel distances along a bundle of MTs is consistent with performances achieved *in vivo*. The motors switch from one MT to another and, in this way reach the extremities of axons. Nevertheless, the systems differ in their dimensionalities and the ability for the motor to dissociate from the cargo. In cells, MTs are spatially organized. Therefore, a detached motor can diffuse in any direction and reattach. In addition, full length kinesins and larger cargos allow more simultaneous bindings, dramatically increasing the run length. In our experiment, the conditions are less favorable, but they still suffice to achieve long travel distances. If we fully control the formation of loops, further trials may allow the identification of the minimal conditions required for long-range transportation.

CONCLUSION

Loops made of MTs constitute unlimited paths for kinesin driven cargos. QD trajectories along a loop have been analyzed. On average, considering micrometer segments, the difference of velocity between QDs is estimated to about 25% of the average velocity. The velocity variations seem highly correlated to the presence of obstacles but a dramatic decrease does not seem mandatory due to the presence of multiple parallel paths. The trajectories were found to be highly similar from one lap to another. The long travel distances may be explained by multiple short runs of the QD. This assay shows that such distances can be achieved by the multiple-motor driven transport using a bundle of a few MTs arranged in unipolar orientation. It may be interesting to continue the long-range transport study on artificially organized MTs. Among different approaches, one can use metallic glass microwires[33] or circular metallic patterns[34] as electrodes to arrange the MTs. Reduction of the electrode width, using for example dielectrophoretically aligned carbon nanotubes,[35] may allow the elaboration of single MT loops.

MATERIALS AND METHODS

Probability of Similarity. Two trajectories are compared in *N* different locations. At each location, one character among three (increasing, decreasing, or local minimum) is conferred. Thus, the comparison of 2 trajectories can be assimilated to the comparison of 2 rows of a *N* columns table in which 3 kinds of item can be inserted (see Figure S5 for the analysis of QD1).

For a table of N columns and 2 rows, the 3 kinds of item can be inserted in 3^{2N} possible ways.

When the item is identical in 1 column, there is a similitude. q is the number of similitudes. The number of configurations in which there are q similitudes, *i.e.*, the number of ways to put q items in N locations, is ${}_NC_q = [N!/q!(N-q)!]$.[36]

In these q columns, the 3 kinds of items can be organized in 3^q different ways.

There are $N - q$ remaining columns in which 2 different items must be inserted. There are two lines so the number of configuration can be doubled. Therefore, the remaining columns have $(2 \times {}_3C_2)^{N-q}$ possible configurations.

Thus, the probability $P(q,N)$ of finding q similitudes in a table of N columns and 2 rows can be written as follows:

$$P(q, N) = \frac{{}_NC_q\, 3^q (2_3C_2)^{N-q}}{3^{2N}} \quad (1)$$

The probability $P(I > q,N)$ to get more than q similitudes at N locations is $\sum_{q+1}^{N} P(i,N)$.

MT and Kinesin. A 7:3 mixture of nonlabeled/rhodamine labeled tubulin was polymerized from commercially available porcine tubulin (Cytoskeleton, USA) according to a protocol described elsewhere.[37]

The kinesin used in the QD assay consists in the 400 first amino acids of *Neurospora crassa*'s kinesin-1 (NCkin) fused with a biotin carboxyl carrier protein (BCCP),[38] a short linker[39] and a hexahistidine tag. NCkin's DNA was purchased from Life Technologies. To insert the NCkin's gene, the pRA2 expression vector was digested with NcoI and SacII enzymes. The NCkin's gene was ligated to the pRA2 vector using a DNA Ligation Kit Mightly mix (TaKaRa Co., Ltd.). The gene sequence was checked with a 3130xl Genetic Analyzer (Applied Biosystems). The gene was then expressed in *Escherichia coli* following a standard protocol.[40]

QD Assay. In this assay, all the solutions are made with BRB80 buffer.[41] First, a regular flow cell[34] was filled with a PLL solution (0.01% w/v) and incubated for 30 min in order to fix the MT on the surface.[25] After the flow cell was washed with 40 μL of BRB80, a microtubule dispersion (tubulin concentration: 2.5 μg/mL) was injected and incubated for 5 min. As a way to prevent QD adsorption on the surface, the chamber was then flushed with a 0.5 mg/mL casein solution complemented with taxol (10 μM) and antifade (20 μg mL^{-1} glucose oxidase, 8 μg mL^{-1} catalase, 20 mM glucose), and incubated for 5 min. Meanwhile, streptavidin coated QDs (about 20 nm in diameter, 100 nM, Invitrogen Ltd. Qdot 655-streptavidin conjugates) and kinesin (0.8 μM) were incubated in a 0.2 mg/mL casein solution, complemented with 1 mM ATP. To finish, a 100× dilution of the QD/kinesin mix in a 0.2 mg/mL casein solution complemented with taxol (10 μM), antifade and 5 mM ATP was injected. After it was sealed with VALAP (1:1:1 vaseline/lanolin/paraffin) to avoid drying, the flow cell was mounted on the microscope stage. The assay was performed at room temperature.

Fluorescence Microscopy. The flow cell was mounted on an inverted microscope IX71 (Olympus, Japan) equipped with a digital CCD camera (Hamamatsu, ImageEM) and a rhodamine filter set (Omega Optical, Inc., XF204). Images were acquired and processed using Metamorph and ImageJ.

Dynamic Light Scattering. DLS measurements were performed 5 times for each sample, using a Zetasizer Nano-ZS (Malvern, U.K.). Samples were composed of 1 nM QD dispersed in 1 mL of BRB80 buffer and mixed with various amounts of kinesin, casein, and PLL.

Trajectory Acquisition Using a Stepper Algorithm. To systematically find and analyze QD trajectories along the microtubule loop in kymographs, we developed our own software. First, a kymograph is constructed from the recorded movie and converted into an $n \times m$ matrix **K**. Each matrix element K_{ij} represents the light intensity measured in frame i at position j along the loop. Both i and j are integer numbers corresponding to the pixel coordinates in the kymograph, which can be converted to time and distance scales, knowing that frames are recorded at 10 frames/s, and a pixel in the j-axis corresponds to a length of 100 nm. The intensity is also normalized so that 1 is the highest recorded brightness. We then interpolate the matrix **K** and obtain a continuous intensity surface I:

$$I(X) = I(x; y) = \mathrm{bilin}(K_{i,j}) \quad (2)$$

where X is a point in kymograph space, at time x and position along the loop y, and the bilin is the bilinear interpolation function. Periodic boundary conditions are enforced along the spatial axis.

The main idea of the software is to walk on the kymograph in the direction where the intensity is highest, as seen in Figure S7. The algorithm scans the kymograph until it finds a bright point $X_1 = (x_1; y_1)$ where $I(X_1) > 0.1$ is found. Below this threshold, the image is too dim to safely assume the presence of a QD track, and the analysis is not reliable. To find the direction of the track, the brightness of the kymograph has to be estimated along all possible directions e_v starting from X_1. We define such an intensity factor as

$$S(X_1, v) = \int_{\gamma(X_1, v)} I(s)\, \mathrm{d}s \quad (3)$$

The integration path $\gamma(X_1, v)$ is the straight line segment along the unitary vector e_v, starting at X_1:

$$\gamma(X_1, v) = X_1 + se_v, s \in [0, s_{\max}] \quad (4)$$

where $s_{\max} = 3$ pixels is chosen so that $\gamma(v)$ is always within the thickness of a QD track. Each direction e_v in kymograph space corresponds to one particular velocity of the QD. It can be seen that the intensity factor S quantifies the kymograph brightness along a specific direction, and the integral smoothens the noise. All results were calculated also for $s_{\max} = 5$, but no significant change was observed. After $S(X_1,v)$ is computed for all $v \in [0; 1000]$ nm/s with a resolution of 1 nm/s, we find the direction $v_{\max}$ that maximizes S, and take a step to $X_2 = X_1 + e_v$. After stepping to the new position X_k, all pixels in the kymograph laying behind the path, *i.e.*, where $x_k - 5 < x < x_k$ and $y_k - 5 \leq y < y_k$ are painted black, to avoid walking multiple times on the same trajectory. The path detection continues as long as $S(X_k; v_{\max})/s_{\max} > 0.1$, *i.e.*, there is a sufficiently bright direction, and X_k is within the time range of the kymograph. When a trajectory ends, all positions x_i and velocities v_i are saved, and the program looks for a new starting point.

Conflict of Interest: The authors declare no competing financial interest.

Supporting Information Available: The Supporting Information is available free of charge on the ACS Publications website at DOI: 10.1021/acsnano.5b04348.

Additional experimental data (figures and tables) (PDF)
Movie S1 (AVI)
Movie S2 (AVI)

Acknowledgment. We gratefully acknowledge support from the World Premier International Research Center Initiative (WPI), MEXT, Japan. We would like to thank Mr. Noguchi Masahiro and Dr. Daisuke Hojo for the DLS measurements, as well as Prof. Izumi Kumagai's students, especially Mr. Aruto Sugiyama, Mr. Takuma Sujino and Ms. Rui Todokoro.

REFERENCES AND NOTES

1. Vale, R. D. The Molecular Motor Toolbox for Intracellular Transport. *Cell* **2003**, *112*, 467–480.
2. Goldstein, L. S. B.; Yang, Z. Microtubule-Based Transport Systems in Neurons: The Roles of Kinesins and Dyneins. *Annu. Rev. Neurosci.* **2000**, *23*, 39–71.
3. Nitzsche, B.; Ruhnow, F.; Diez, S. Quantum-Dot-Assisted Characterization of Microtubule Rotations During Cargo Transport. *Nat. Nanotechnol.* **2008**, *3*, 552–6.
4. Alushin, G. M.; Lander, G. C.; Kellogg; Elizabeth, H.; Zhang, R.; Baker, D.; Nogales, E. High-Resolution Microtubule Structures Reveal the Structural Transitions in Aβ-Tubulin Upon Gtp Hydrolysis. *Cell* **2014**, *157*, 1117–1129.
5. Ray, S.; Meyhöfer, E.; Milligan, R. A.; Howard, J. Kinesin Follows the Microtubule's Protofilament Axis. *J. Cell Biol.* **1993**, *121*, 1083–1093.

6. Yildiz, A.; Tomishige, M.; Gennerich, A.; Vale, R. D. Intramolecular Strain Coordinates Kinesin Stepping Behavior Along Microtubules. *Cell* **2008**, *134*, 1030–41.
7. Seitz, A.; Surrey, T. Processive Movement of Single Kinesins on Crowded Microtubules Visualized Using Quantum Dots. *EMBO J.* **2006**, *25*, 267–277.
8. Telley, I. A.; Bieling, P.; Surrey, T. Obstacles on the Microtubule Reduce the Processivity of Kinesin-1 in a Minimal in Vitro System and in Cell Extract. *Biophys. J.* **2009**, *96*, 3341–53.
9. Dreblow, K.; Kalchishkova, N.; Böhm, K. J. Kinesin Passing Permanent Blockages Along Its Protofilament Track. *Biochem. Biophys. Res. Commun.* **2010**, *395*, 490–495.
10. Ray, K. How Kinesins Walk, Assemble and Transport: A Birds-Eye-View of Some Unresolved Questions. *Phys. A* **2006**, *372*, 52–64.
11. Block, S. M.; Goldstein, L. S. B.; Schnapp, B. J. Bead Movement by Single Kinesin Molecules Studied with Optical Tweezers. *Nature* **1990**, *348*, 348–352.
12. Coy, D. L.; Wagenbach, M.; Howard, J. Kinesin Takes One 8-Nm Step for Each Atp That It Hydrolyzes. *J. Biol. Chem.* **1999**, *274*, 3667–3671.
13. Beeg, J.; Klumpp, S.; Dimova, R.; Gracia, R. S.; Unger, E.; Lipowsky, R. Transport of Beads by Several Kinesin Motors. *Biophys. J.* **2008**, *94*, 532–41.
14. Böhm, K. J.; Stracke, R.; Mühlig, P.; Unger, E. Motor Protein-Driven Unidirectional Transport of Micrometer-Sized Cargoes across Isopolar Microtubule Arrays. *Nanotechnology* **2001**, *12*, 238.
15. Korn, C. B.; Klumpp, S.; Lipowsky, R.; Schwarz, U. S. Stochastic Simulations of Cargo Transport by Processive Molecular Motors. *J. Chem. Phys.* **2009**, *131*, 245107.
16. Klumpp, S.; Lipowsky, R. Cooperative Cargo Transport by Several Molecular Motors. *Proc. Natl. Acad. Sci. U. S. A.* **2005**, *102*, 17284–9.
17. Muthukrishnan, G.; Hutchins, B. M.; Williams, M. E.; Hancock, W. O. Transport of Semiconductor Nanocrystals by Kinesin Molecular Motors. *Small* **2006**, *2*, 626–30.
18. Vershinin, M.; Carter, B. C.; Razafsky, D. S.; King, S. J.; Gross, S. P. Multiple-Motor Based Transport and Its Regulation by Tau. *Proc. Natl. Acad. Sci. U. S. A.* **2007**, *104*, 87–92.
19. Xu, J.; Shu, Z.; King, S. J.; Gross, S. P. Tuning Multiple Motor Travel Via Single Motor Velocity. *Tra□c* **2012**, *13*, 1198–1205.
20. Rogers, A. R.; Driver, J. W.; Constantinou, P. E.; Kenneth Jamison, D.; Diehl, M. R. Negative Interference Dominates Collective Transport of Kinesin Motors in the Absence of Load. *Phys. Chem. Chem. Phys.* **2009**, *11*, 4882–4889.
21. Kakugo, A.; Kabir, A. M.; Hosoda, N.; Shikinaka, K.; Gong, J. P. Controlled Clockwise-Counterclockwise Motion of the Ring-Shaped Microtubules Assembly. *Biomacromolecules* **2011**, *12*, 3394–9.
22. Liu, L.; Tuzel, E.; Ross, J. L. Loop Formation of Microtubules During Gliding at High Density. *J. Phys.: Condens. Matter* **2011**, *23*, 374104.
23. Bachand, M.; Trent, A. M.; Bunker, B. C.; Bachand, G. D. Physical Factors Affecting Kinesin-Based Transport of Synthetic Nanoparticle Cargo. *J. Nanosci. Nanotechnol.* **2005**, *5*, 718–722.
24. Inoue, D.; Kabir, A. M. R.; Mayama, H.; Gong, J. P.; Sada, K.; Kakugo, A. Growth of Ring-Shaped Microtubule Assemblies through Stepwise Active Self-Organisation. *Soft Matter* **2013**, *9*, 7061.
25. Yokokawa, R.; Takeuchi, S.; Kon, T.; Nishiura, M.; Ohkura, R.; Edamatsu, M.; Sutoh, K.; Fujita, H. Hybrid Nanotransport System by Biomolecular Linear Motors. J. *J. Microelectromech. Syst.* **2004**, *13*, 612–619.
26. Stracke, R.; Böhm, K. J.; Burgold, J.; Schacht, H.-J.; Unger, E. Physical and Technical Parameters Determining the Functioning of a Kinesin-Based Cell-Free Motor System. *Nanotechnology* **2000**, *11*, 52.
27. Sikora, A.; Oliveira, D.; Kim, K.; Liao, A. L.; Umetsu, M.; Kumagai, I.; Adschiri, T.; Hwang, W.; Teizer, W. Quantum Dot Motion on Microtubules. *Chem. Lett.* **2012**, *41*, 1215–1217.
28. Conway, L.; Wood, D.; Tüzel, E.; Ross, J. L. Motor Transport of Self-Assembled Cargos in Crowded Environments. *Proc. Natl. Acad. Sci. U. S. A.* **2012**, *109*, 20814–20819.
29. Kunwar, A.; Mogilner, A. Robust Transport by Multiple Motors with Nonlinear Force-Velocity Relations and Stochastic Load Sharing. *Phys. Biol.* **2010**, *7*, 16012.
30. Horne, D. S. Casein Structure, Self-Assembly and Gelation. *Curr. Opin. Colloid Interface Sci.* **2002**, *7*, 456–461.
31. O'Connell, J. E.; Grinberg, V. Y.; de Kruif, C. G. Association Behavior of B-Casein. *J. Colloid Interface Sci.* **2003**, *258*, 33–39.
32. Woehlke, G.; Ruby, A. K.; Hart, C. L.; Ly, B.; Hom-Booher, N.; Vale, R. D. Microtubule Interaction Site of the Kinesin Motor. *Cell* **1997**, *90*, 207–216.
33. Kim, K.; Sikora, A.; Nakayama, K. S.; Nakazawa, H.; Umetsu, M.; Hwang, W.; Teizer, W. Functional Localization of Kinesin/Microtubule-Based Motility System Along Metallic Glass Microwires. *Appl. Phys. Lett.* **2014**, *105*, 143701.
34. Noel, J. A.; Teizer, W.; Hwang, W. Surface Manipulation of Microtubules Using Self-Assembled Monolayers and Electrophoresis. *ACS Nano* **2009**, *3*, 1938–1946.
35. Sikora, A.; Ramón-Azcón, J.; Kim, K.; Reaves, K.; Nakazawa, H.; Umetsu, M.; Kumagai, I.; Adschiri, T.; Shiku, H.; Matsue, T.; et al. Molecular Motor-Powered Shuttles Along Multi-Walled Carbon Nanotube Tracks. *Nano Lett.* **2014**, *14*, 876–881.
36. Mendenhall, W.; Beaver, R. J.; Beaver, B. M. *Introduction to Probability and Statistics*; Brooks/Cole: Belmont, CA, 2012.
37. Maloney, A.; Herskowitz, L. J.; Koch, S. J. Effects of Surface Passivation on Gliding Motility Assays. *PLoS One* **2011**, *6*, e19522.
38. Kim, D.-M.; Umetsu, M.; Takai, K.; Matsuyama, T.; Ishida, N.; Takahashi, H.; Asano, R.; Kumagai, I. Enhancement of Cellulolytic Enzyme Activity by Clustering Cellulose Binding Domains on Nanoscaffolds. *Small* **2011**, *7*, 656–664.
39. Cloutier, S. M.; Couty, S.; Terskikh, A.; Marguerat, L.; Crivelli, V.; Pugnières, M.; Mani, J. C.; Leisinger, H. J.; Mach, J. P.; Deperthes, D. Streptabody, a High Avidity Molecule Made by Tetramerization of in Vivo Biotinylated, Phage Display-Selected Scfv Fragments on Streptavidin. *Mol. Immunol.* **2000**, *37*, 1067–1077.
40. Oliveira, D.; Kim, D. M.; Umetsu, M.; Kumagai, I.; Adschiri, T.; Teizer, W. The Assembly of Kinesin-Based Nanotransport Systems. *J. Appl. Phys.* **2012**, *112*, 124703.
41. Olmsted, J. B.; Borisy, G. G. Ionic and Nucleotide Requirements for Microtubule Polymerization in Vitro. *Biochemistry* **1975**, *14*, 2996–3005.
42. Jon Kull, F.; Sablin, E. P.; Lau, R.; Fletterick, R. J.; Vale, R. D. Crystal Structure of the Kinesin Motor Domain Reveals a Structural Similarity to Myosin. *Nature* **1996**, *380*, 550–555.
43. Balavoine, F.; Schultz, P.; Richard, C.; Mallouh, V.; Ebbesen, T. W.; Mioskowski, C. Helical Crystallization of Proteins on Carbon Nanotubes: A First Step Towards the Development of New Biosensors. *Angew. Chem., Int. Ed.* **1999**, *38*, 1912–1915.
44. Pampaloni, F.; Florin, E. L. Microtubule Architecture: Inspiration for Novel Carbon Nanotube-Based Biomimetic Materials. *Trends Biotechnol.* **2008**, *26*, 302–10.

Supporting information

Behavior of Kinesin Driven Quantum Dots Trapped in a Microtubule Loop

Aurélien Sikora,[†] Filippo Federici Canova,[†] Kyongwan Kim,[†] Hikaru Nakazawa,[‡] Mitsuo Umetsu,[‡] Izumi Kumagai,[‡] Tadafumi Adschiri,[†] Wonmuk Hwang,[§,□,Δ] Winfried Teizer[†,Δ,○]

[†] WPI Advanced Institute for Materials Research, Tohoku University, 2-1-1 Katahira, Sendai, 980-8577, Japan

[‡] Department of Biomolecular Engineering, Graduate School of Engineering, Tohoku University, Sendai 980-8579, Japan

[§] Department of Biomedical Engineering, Texas A&M University, College Station, TX 77843-3120, USA

[□] School of Computational Sciences, Korea Institute for Advanced Study, Seoul, 130-722, Korea

[Δ] Materials Science and Engineering, Texas A&M University, College Station, TX 77843-3003, USA

[○] Department of Physics and Astronomy, Texas A&M University, College Station, TX 77843-4242, USA

Movie 1: Kinesin driven QDs moving along a MT loop. The ratio between kinesin and QDs was 8. Final concentrations: 8 nM for kinesin, 1 nM for QDs. Real time duration: 5 mn. Replay rate: 5 times normal speed. Size: 9.7 x 13.3 µm.

Movie 2: Kinesin driven QDs moving along an antiparallel bundle of MT. The ratio between kinesin and QDs was 1. Final concentrations: 1 nM for kinesin and QDs. Real time duration: 150.5 s. Replay rate: 15 times normal speed. Size: 16.6 x 18.4 µm

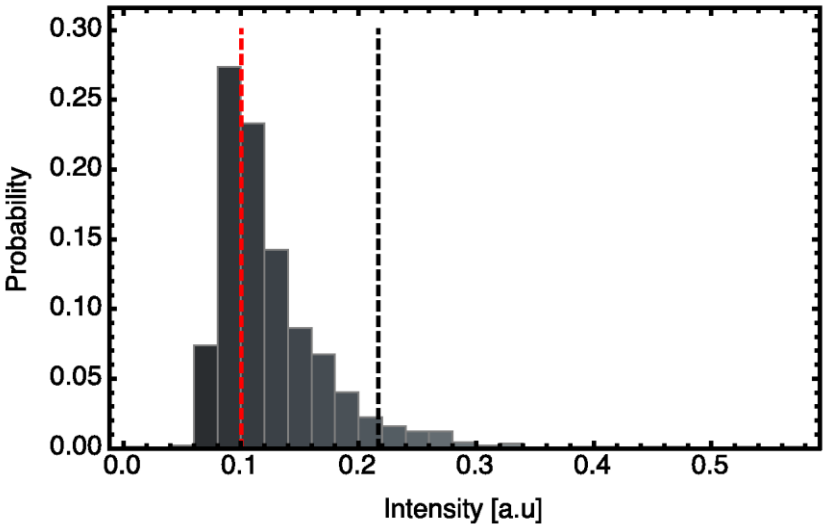

Figure S1. Average intensity distribution of the detected trajectories. The red and black vertical lines show the limits where the cumulative distribution reaches 50% and 95% of the total number of trajectories, respectively.

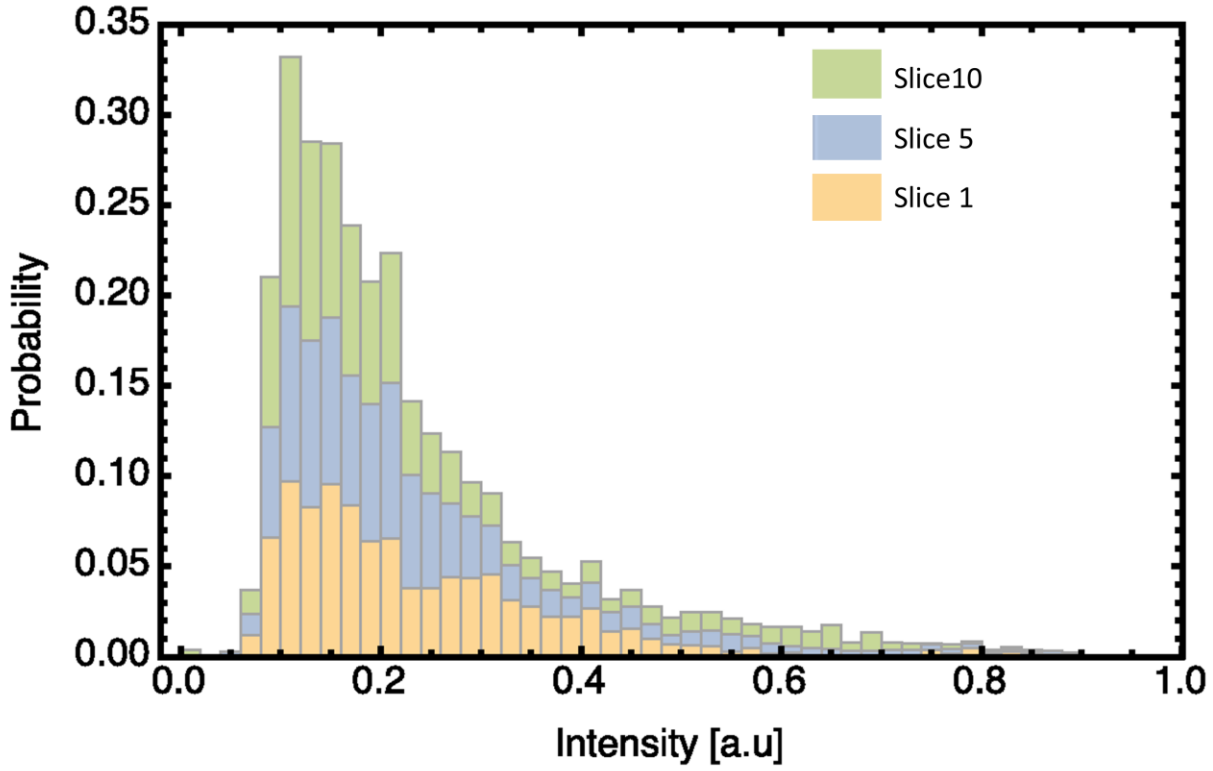

Figure S2. Averaged intensity distribution of the detected trajectories for three different times. The 5 minutes duration of the experiment has been divided into 10 slices. The intensity of a trajectory has been averaged along one slice. The total length of each bar corresponds to the sum of 3 datasets (slices 1, 5 and 10).

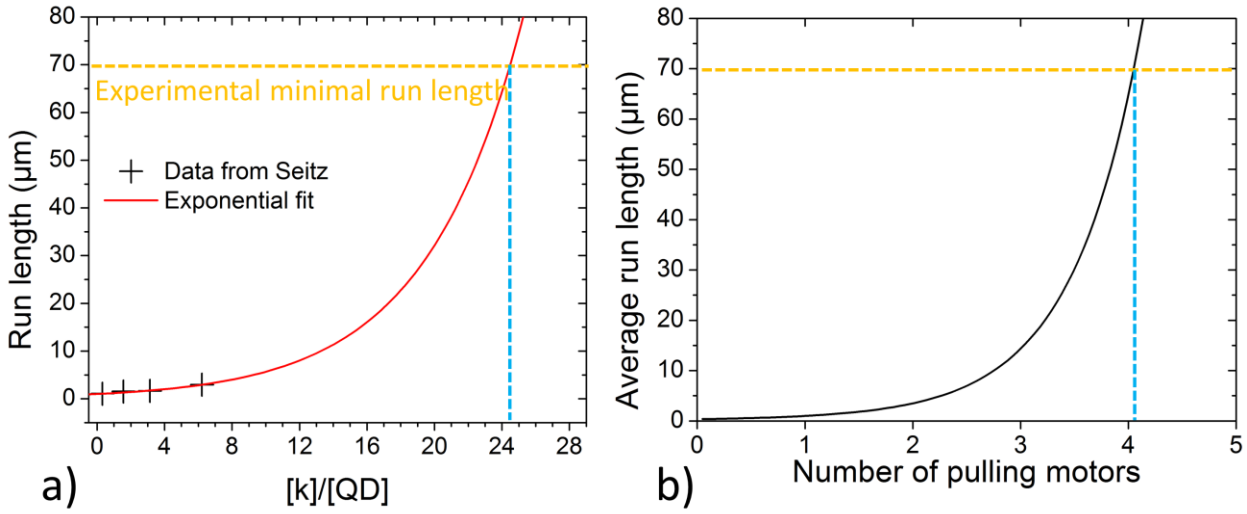

Figure S3. a) Average run length as a function of the ratio between kinesin and QD concentration.[1] Data from Seitz and Surrey have been fitted with an exponential function using Origin Pro software. b) Evolution of the run length with the number of pulling motors according to the equation $d = 6^{N-1}/5N$, with d the run length and N the number of pulling motors, coming from the cooperative model.[2]

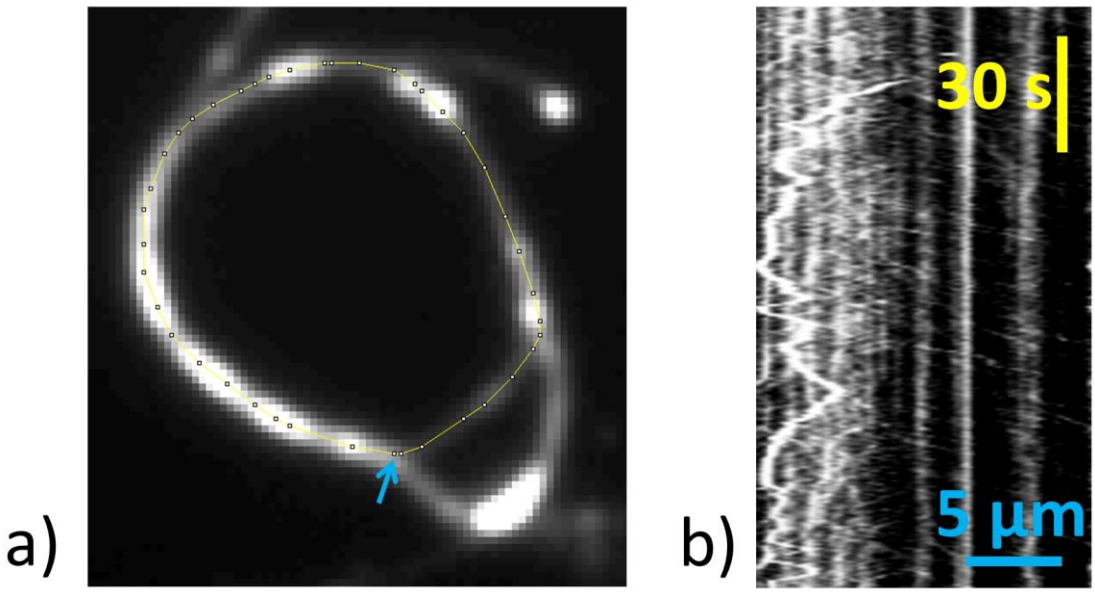

Figure S4. a) Average intensity image of Movie 2 showing the motion of kinesin driven QDs along an antiparallel bundle of MT. The arrow indicates the starting point of the path, which corresponds to the left side of the kymograph. The path (yellow line) is 17.4 µm long. b) Kymograph extracted from the movie 2. Bidirectional motion can be seen on the left side.

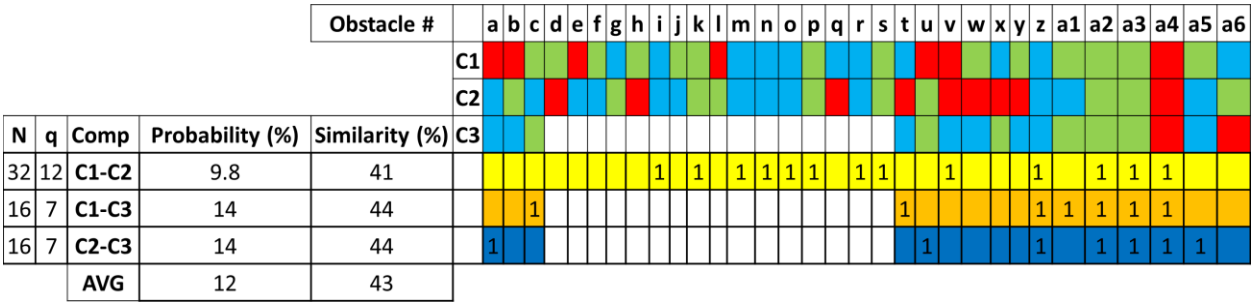

N	q	Comp	Probability (%)	Similarity (%)
32	12	C1-C2	9.8	41
16	7	C1-C3	14	44
16	7	C2-C3	14	44
		AVG	12	43

Figure S5. Example of similarity calculation based on the data from QD1. For each obstacle, the QD velocity is either increasing (red), decreasing (blue) or minimized (green). The cycles are compared by enumerating the number of similitudes. For example, considering obstacle "a", the QD velocity is minimized in cycle 2 and 3. This counts as a similitude. The similarity between two cycles is then given by the ratio between the number of similitude q and the number of common obstacles N. The probability to get q similitudes in N locations has been calculated in the case of a random behavior, i.e. for each obstacle, the QD has a 1/3 probability to be in an increasing phase, decreasing phase or in a state of minimized velocity (see text).

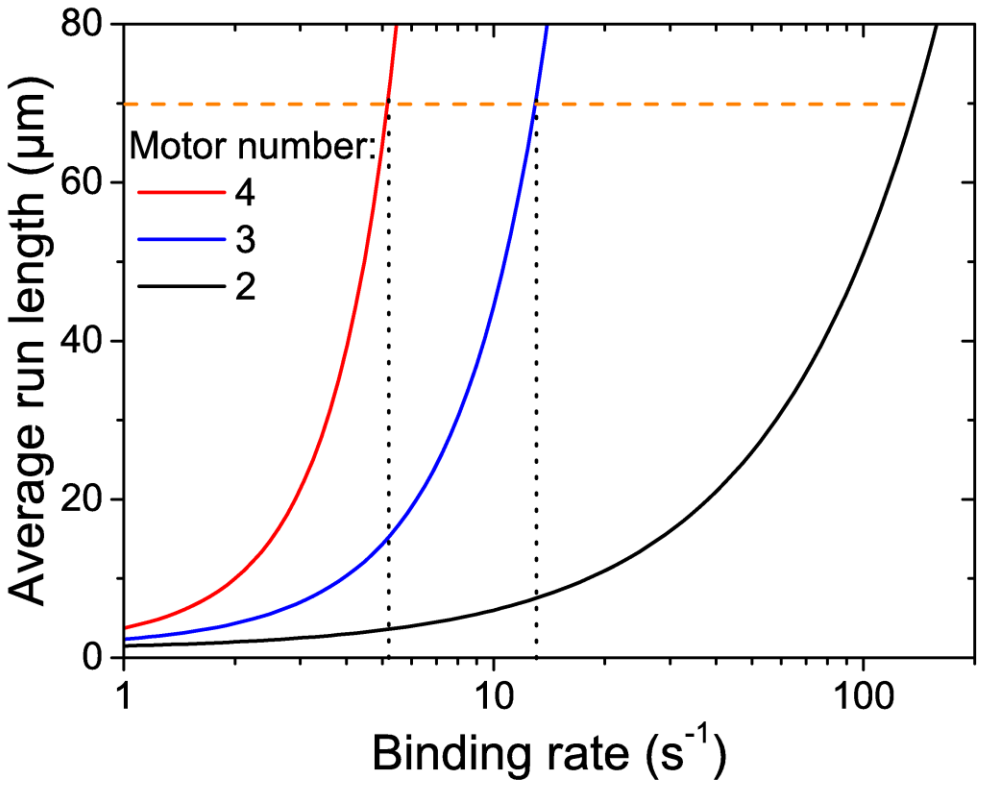

Figure S6. Average run length as a function of the binding rate for a cargo pulled by $N = 2$, 3 and 4 kinesin motors, according to the mean-field theory.[2] Used parameters: velocity $v = 1$ μm s^{-1}, unbinding rate $\varepsilon = 1$ s^{-1}.

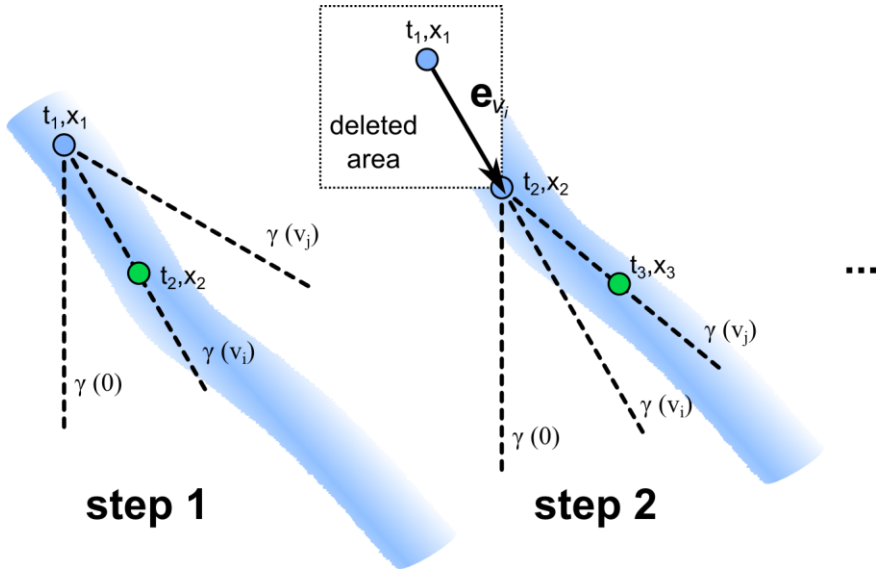

Figure S7. Schematic representation of the analysis algorithm. The kymograph intensity is evaluated along different directions γ(v), and a step is taken along the brightest one. Afterwards, the square area behind the new point is deleted to prevent further walking along the same path.

Table S1. Density of closed MT structures before and after insertion of QD conjugates.

Tubulin concentration ($\mu g\ mL^{-1}$)	2.5	5	10
Density before QD conjugates insertion (mm^{-2})	3	11	23
Density after QD conjugates insertion (mm^{-2})	66	MT network formation	

Table S2. For each visible obstacle, probabilities of the velocity to be a local minimum (Min), to be in a decreasing phase (↘) or to be in an increasing phase (↗).

		Min (%)	**↘ (%)**	**↗ (%)**
QD1	**C1**	43.75	34.38	21.88
	C2	31.25	40.63	28.13
	C3	37.5	50	12.5
QD4	**C1**	37.5	28.13	34.38
	C2	31.25	43.75	25
	C3	44.44	22.22	33.33
	AVG	37.62	36.52	25.87

Table S3. Similarity between QD trajectories. *N* is the number of defects where the comparison has been made. *q* is the number of defects where the behavior is identical. The probability estimates the chance to get the same configuration.

QD#	Comparison	N	q	Probability (%)	Similarity (%)
1	C1/C2	32	13	9.8	41
	C1/C3	16	7	14	44
	C2/C3	16	7	14	44
2	C1/C2	32	17	1.0	53
	C1/C3	9	3	27	33
	C2/C3	9	5	10	56
3	C1/C2	32	20	0.050	63
	C1/C3	17	6	20	35
	C2/C3	17	7	15	41
4	C1/C2	32	14	6.7	44
	C1/C3	18	7	17	39
	C2/C3	18	11	1.1	61
5	C1/C2	32	14	6.7	45
	C1/C3	4	3	9.9	75
	C2/C3	4	3	9.9	75
6	C1/C2	32	13	9.8	42
	C1/C3	9	3	27	33
	C2/C3	9	7	0.73	78

Table S4. Gaussian fit parameters (width *w*, standard deviation *σ*, full width at half maxiumum and height) extracted from Figure 7b.

Profile	w (nm)	σ (nm)	FWHM (nm)	Height (nm)
1	318	159	375	39.8
2	341	170	401	25.5
3	332	166	391	35.4
4	320	160	376	39.8
5	305	152	359	7.22
6	295	147	347	13.3
7a	305	153	359	33.3
7b	431	215	507	14

References

1. Seitz, A.; Surrey, T., Processive Movement of Single Kinesins on Crowded Microtubules Visualized Using Quantum Dots. *EMBO J.* **2006,** *25*, 267-277.
2. Klumpp, S.; Lipowsky, R., Cooperative Cargo Transport by Several Molecular Motors. *Proc. Natl. Acad. Sci. U. S. A.* **2005,** *102*, 17284-9.